
Figures and figure supplements

Allosteric mechanism of signal transduction in the two-component system histidine kinase PhoQ

Brak Mensa *et al*

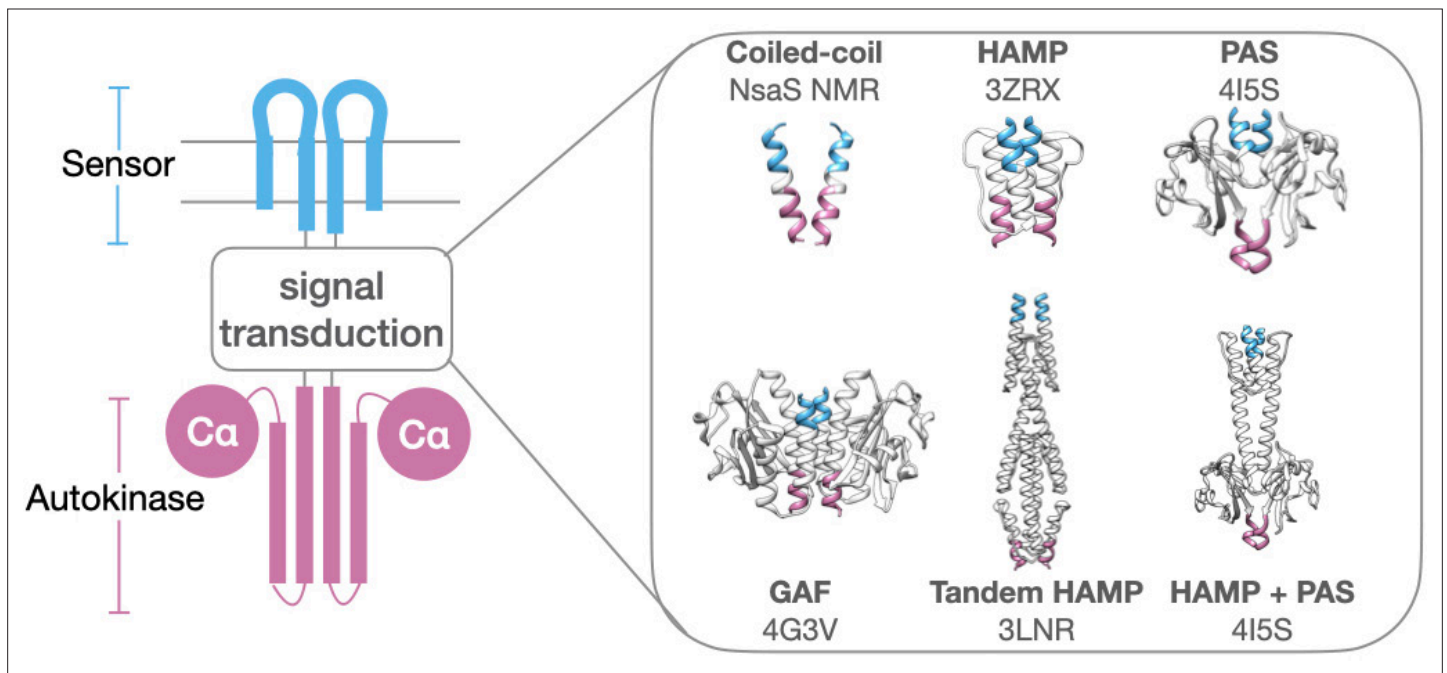


Figure 1. Modular architecture of histidine kinases. Various protein folds and numbers of signal transduction domains are found inserted between sensor (blue) and autokinase (purple). Structurally elucidated examples include simple coiled-coils (NsaS), HAMP (AF1503), PAS (Vick), GAF (Nlh2), Tandem HAMP (Aer2), and HAMP/PAS domain (Vick). PDB codes are provided in figure, except for NsaS (NMR structure).

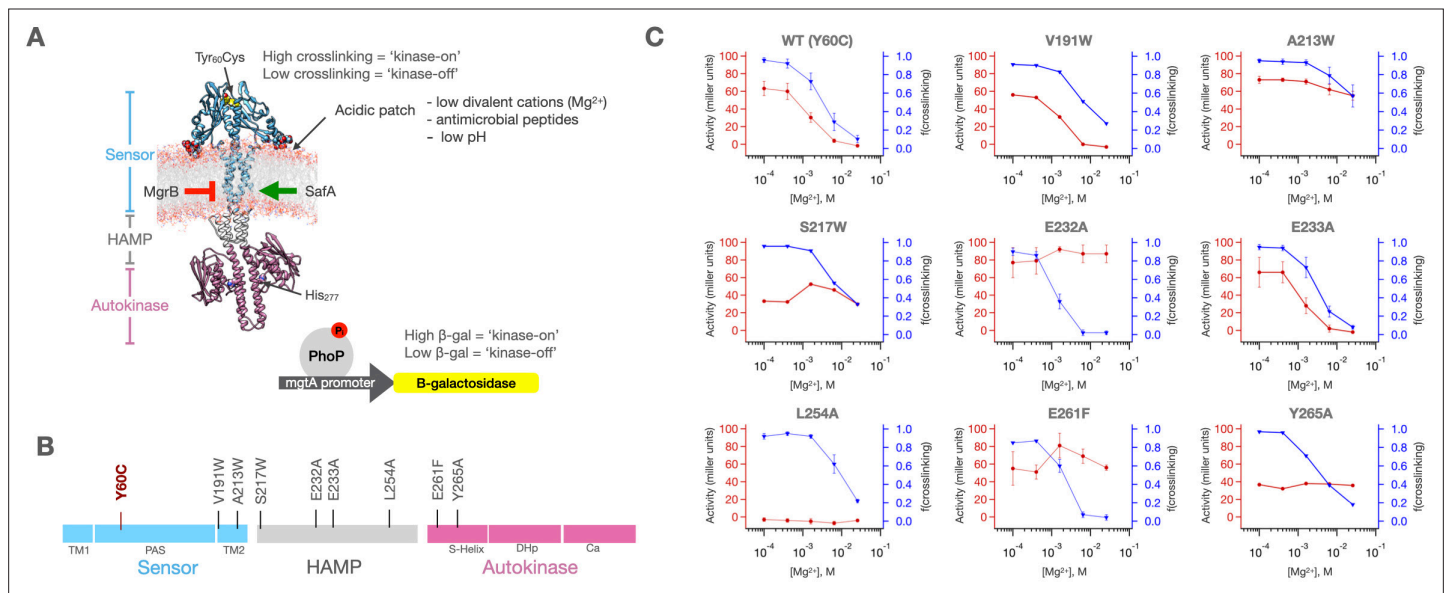


Figure 2. PhoQ single mutants exhibit a range of behaviors. **(A)** Molecular Dynamics model of dimeric PhoQ in which the sensor (res. 1–219, blue), HAMP (res. 220–260, grey) and autokinase domains (res. 261–494, purple) are annotated. The sensor contains a Y60C mutation (spheres) which shows signal state dependent crosslinking. The autokinase contains the conserved catalytic His277, which upon phosphorylation transfers a phosphoryl group to the response regulator PhoP, which then modulates a *mgtA* promoter-driven β -galactosidase reporter. Stimuli and regulatory proteins that modulate PhoQ activity are shown. **(B)** Linear topology diagram of PhoQ. The sensor, HAMP and Autokinase domains are highlighted in blue, gray, and purple, respectively. The locations of mutations in panel (C) are shown. **(C)** fraction of sensor crosslinking (blue) and autokinase activity (red) determined for 'wild type' (Y60C) PhoQ, as well as eight mutants along the signal transduction pathway ($n = 9$ for WT, $n = 2$ for A213W, E232A, E233A, L254A, and E261F, $n = 1$ for V191W, S217W, and Y265A). The sensor state and autokinase activity do not show identical ligand-dependent behavior as would be predicted by a concerted signaling mechanism. Error bars correspond to \pm SD, where applicable.

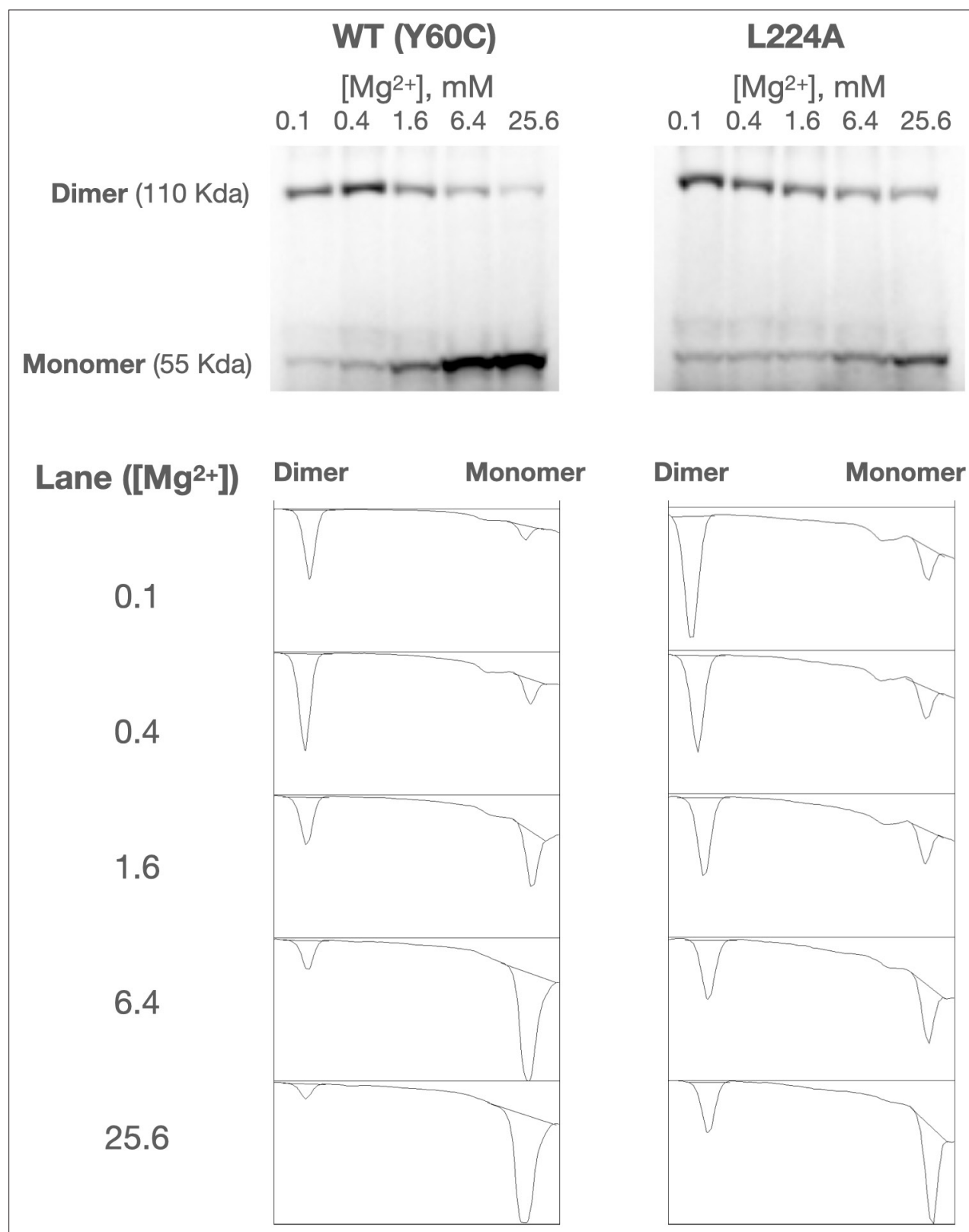


Figure 2—figure supplement 1. Representative PhoQ crosslinking western blot and quantification of WT (Y60C) and Y60C/L224A mutant. LDS buffer solubilized membrane samples are separated by SDS-PAGE and western blotted using an anti-pentaHis antibody. Relative amounts of dimeric and monomeric PhoQ are measured to generate a crosslinking efficiency between 0 and 1.

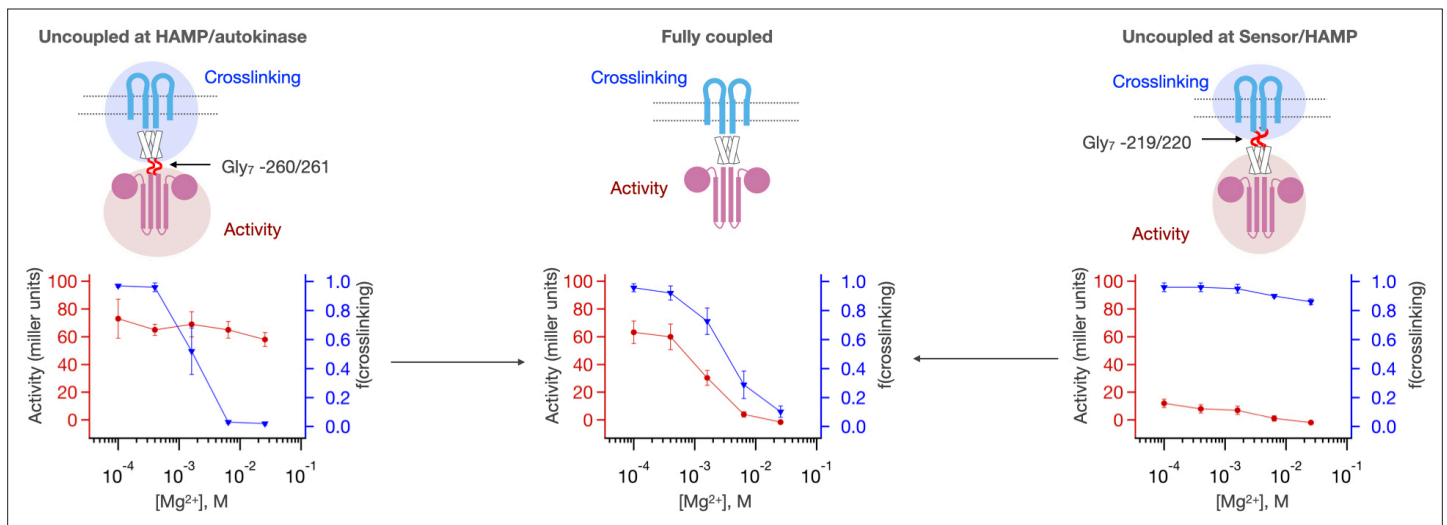


Figure 3. Intrinsic activities of the PhoQ sensor and autokinase domains are altered by coupling to HAMP. Gly₇ insertions are introduced either between the HAMP domain and the autokinase (Gly₇ -260/261, left, n = 3) or between the Sensor and HAMP domain (Gly₇ -219/220, right, n = 2) to disrupt allosteric coupling between sensor and autokinase. Both the sensor and autokinase by themselves show high 'kinase-on' propensity (red trace, left; blue trace, right). The HAMP domain potentiates the 'kinase-off' state, resulting in a more [Mg²⁺] responsive sensor (blue trace, left), or a lower basal activity autokinase (red trace, right). The fully coupled protein shows correlated sensor/autokinase activity (red and blue traces, middle, n = 9).

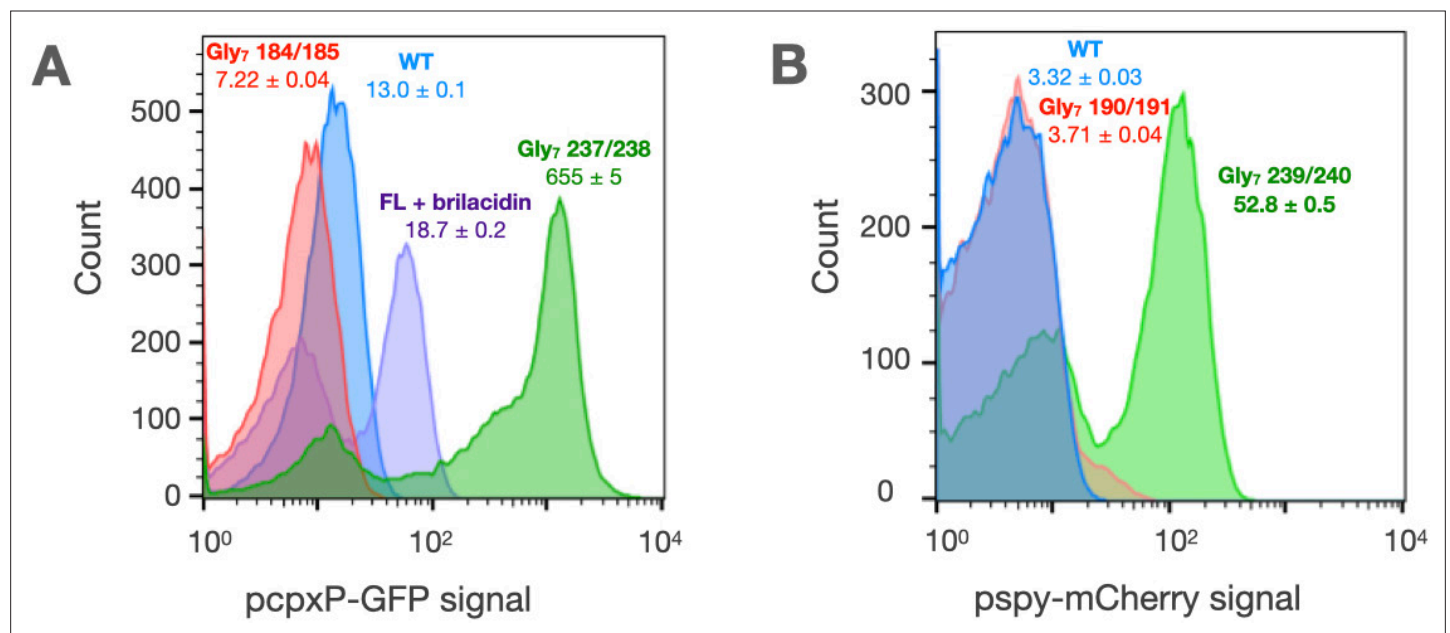


Figure 4. Glycine disconnections in CpxA and BaeS. **(A)** The activity of CpxA constructs is measured in AFS51 strain ($\Delta cpxA$) using a *pcpXP::GFP* reporter. The activity of WT CpxA (blue) is responsive to the antimicrobial mimetic, brilacidin (*Scott et al., 2008; Mensa et al., 2011*) (purple). The autokinase domain of CpxA when uncoupled (Gly₇ 237/238) shows very high kinase activity (green), which is repressed to basal levels by the addition of the HAMP domain alone (Gly₇ 184/185, red). **(B)** The activity of BaeS constructs is measured in a $\Delta baeS \Delta cpxA$ strain using a *pspy::mCherry* reporter. The autokinase domain of BaeS when uncoupled shows high kinase activity (Gly₇ 239/240, green) relative to WT (blue), which is repressed by the addition of the HAMP domain alone (Gly₇ 190/191, red). Median reporter fluorescence values \pm STE ($n = 20,000$) are reported below labels for single experiment.

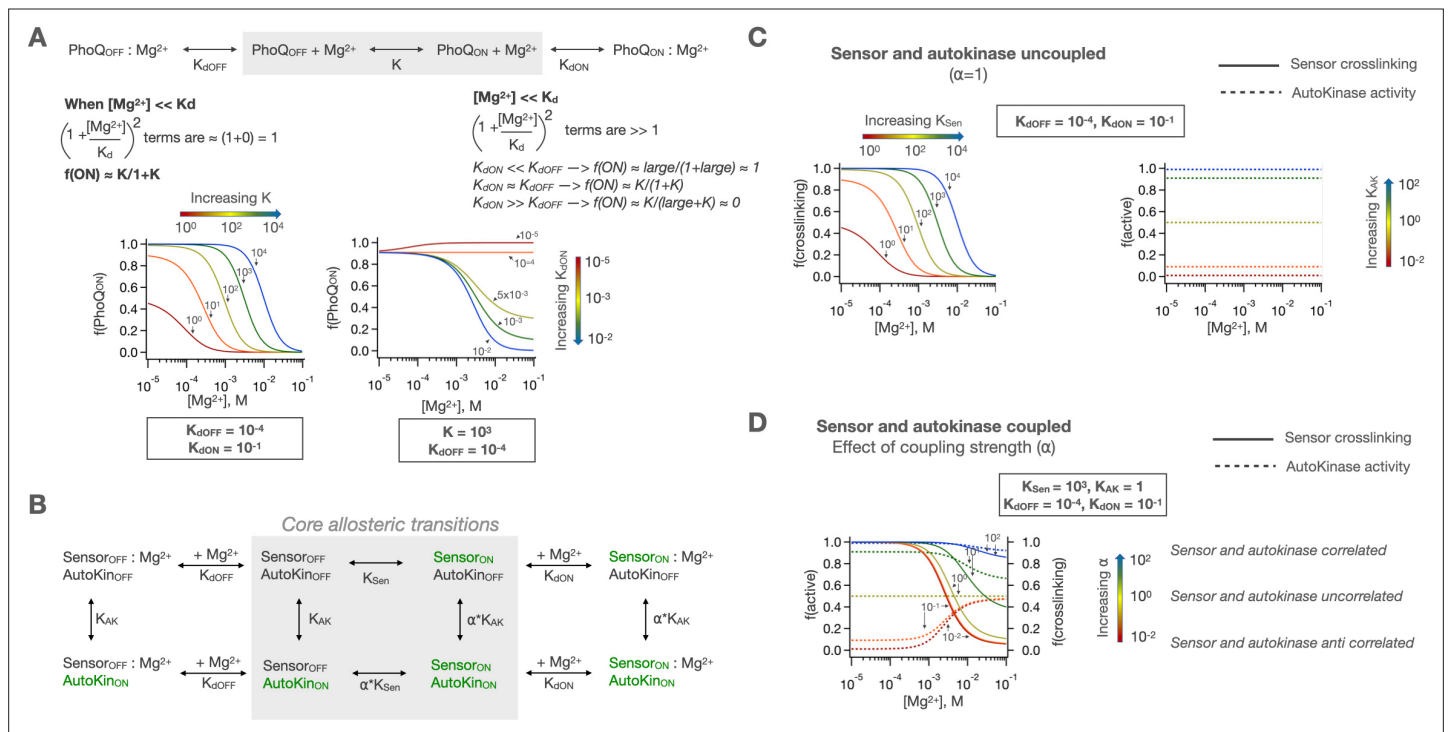


Figure 5. Concerted and two-domain allosteric models for PhoQ signaling. **(A)** In a concerted model for signaling, PhoQ has an intrinsic on-off equilibrium (constant = K) which is modulated by Mg²⁺ binding to either states with corresponding K_ds. This allows for modulation of both low and high activity asymptotes and the midpoint of transition but requires perfect correlation between sensor and autokinase signaling states. Equations for calculating population fractions are shown in Methods (**Equation 1**). **(B)** The sensor and autokinase domains of PhoQ are allowed to sample both 'kinase-on' and 'kinase-off' states with equilibrium constants K_{Sen} and K_{AK} when the other domain is in the 'kinase-off' state. When the other domain is in the 'kinase-on' state, the equilibria are scaled by the coupling constant, α. This allows for semi-independent fractions of sensor and autokinase in the 'kinase-on' state, which are computed as shown in Methods (**Equation 2**). **(C)** In the uncoupled case (α = 1), K_{Sen} modulates the sensor identically to the previously described concerted signaling mechanism, while K_{AK} sets the basal autokinase activity. **(D)** The coupling of these domains with α ≠ 1 results in [Mg²⁺] dependent activity that is either correlated (α > 1) or anticorrelated (α < 1). As α gets larger, the two domains act more as one concerted protein.

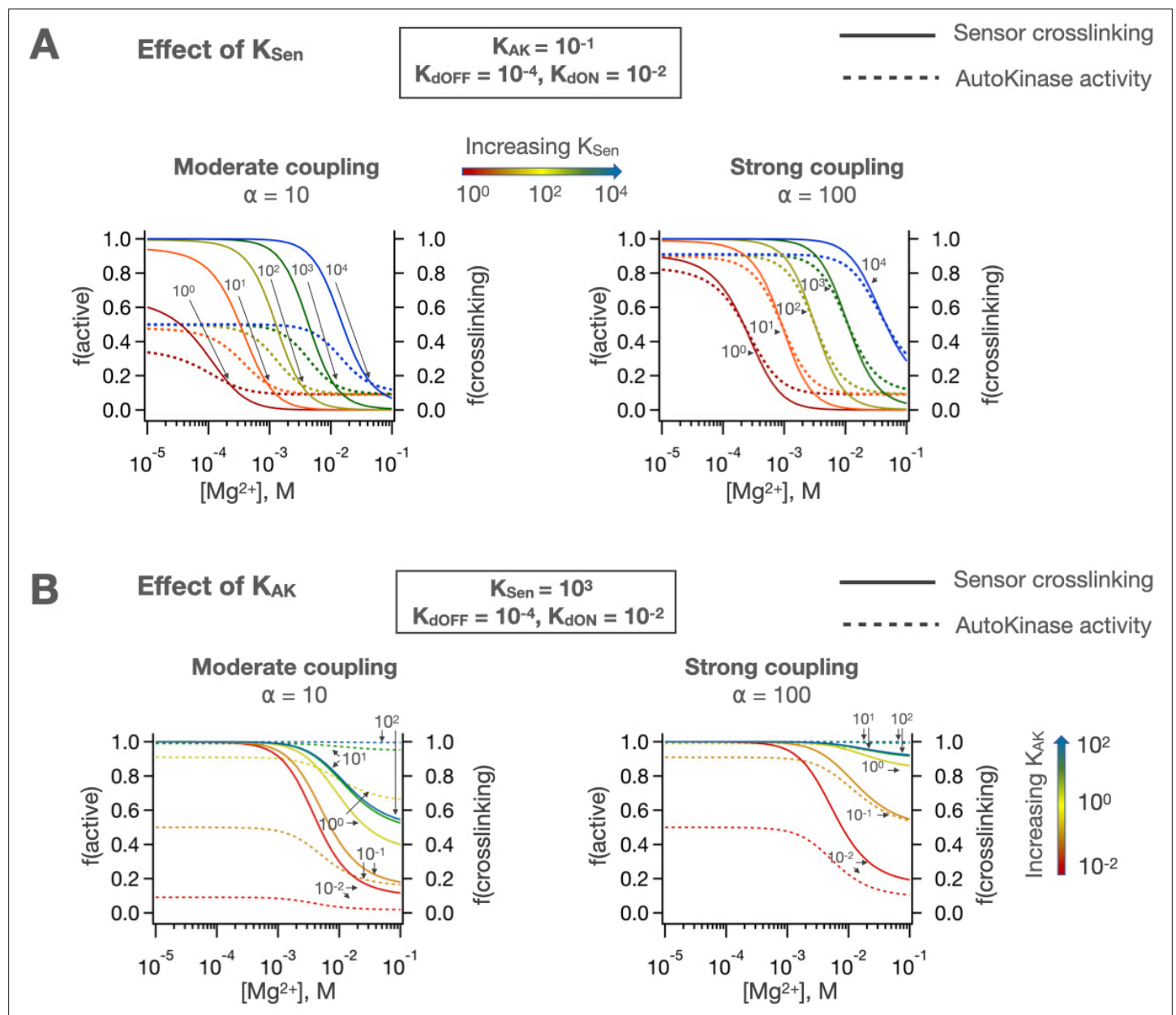
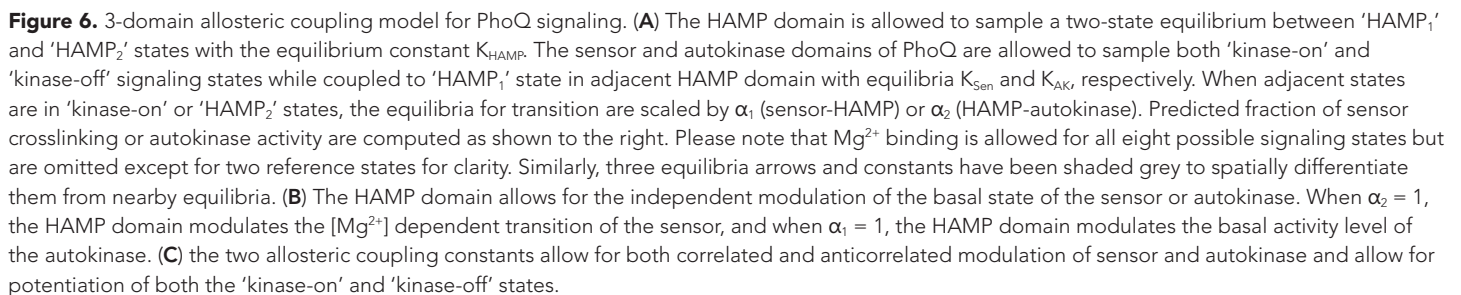


Figure 5—figure supplement 1. Effects of K_{Sen} and K_{AK} on two-domain signaling. (A) Changes in the intrinsic equilibrium of the sensor affect autokinase activity through coupling, and similarly (B) changes in the intrinsic equilibrium of the autokinase domain can alter the ligand-dependent crosslinking behavior of the sensor.



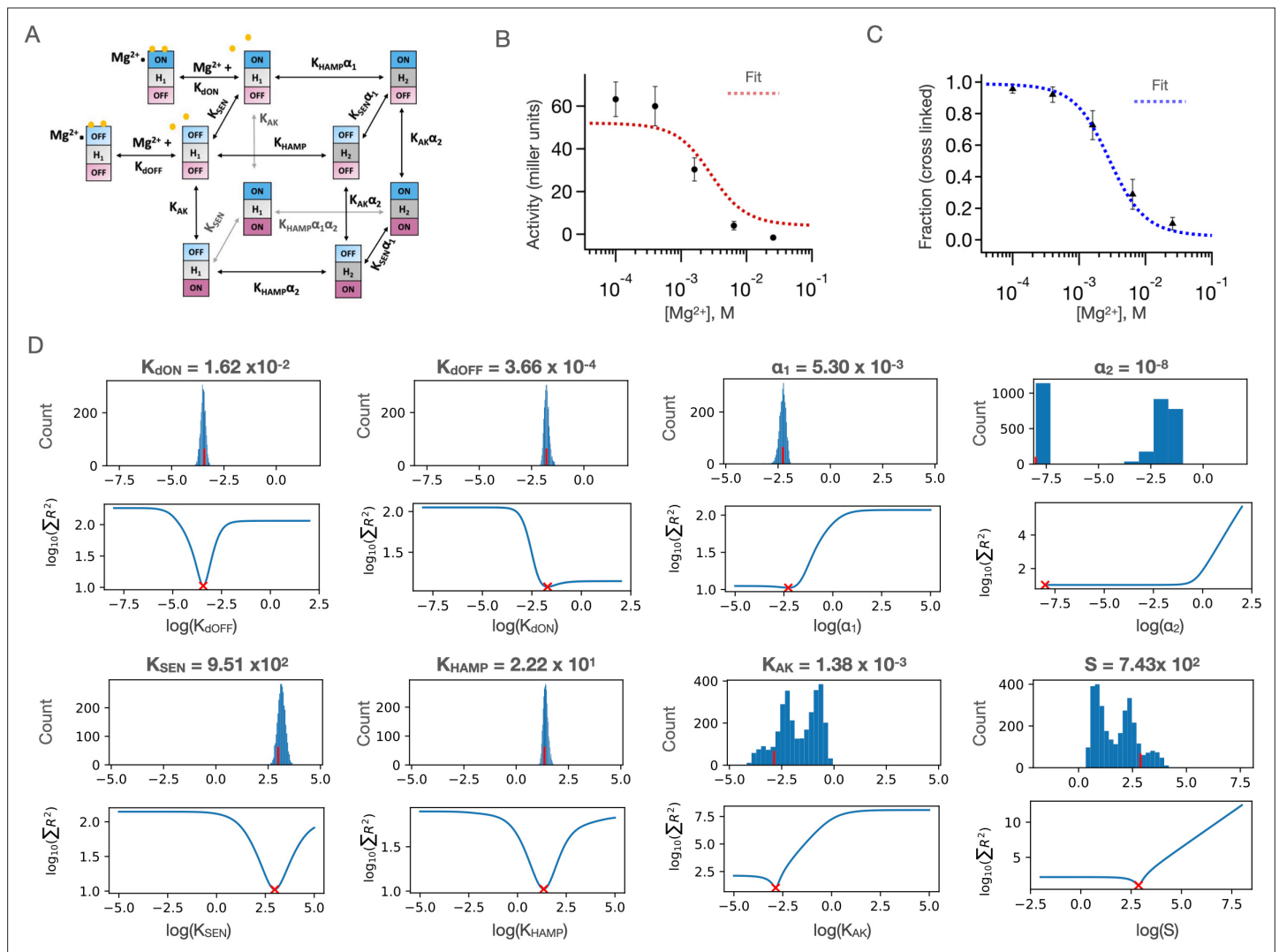


Figure 7. Results of three-domain two-state allosteric model fit of PhoQ activity. **(A)** Three-domain two-state allosteric model used for fitting (see also **Figure 6A**) **(B)** Fits to the $[Mg^{2+}]$ -dependent kinase activity and **(C)** sensor crosslinking for 'wild type' Y60C PhoQ are shown. Error bars correspond to \pm SD for $n = 9$ biological replicates. **(D)** Bootstrapped confidence intervals (top) and residual sweep analyses (bottom) are shown for all eight global parameters. The value of the fit is indicated with red (x) and (|) marks. The confidence intervals of parameters S , K_{AK} and α_2 are further parsed in **Figure 7—figure supplement 2**, and the confidence intervals for α_2 are further parsed in **Figure 7—figure supplement 3**.

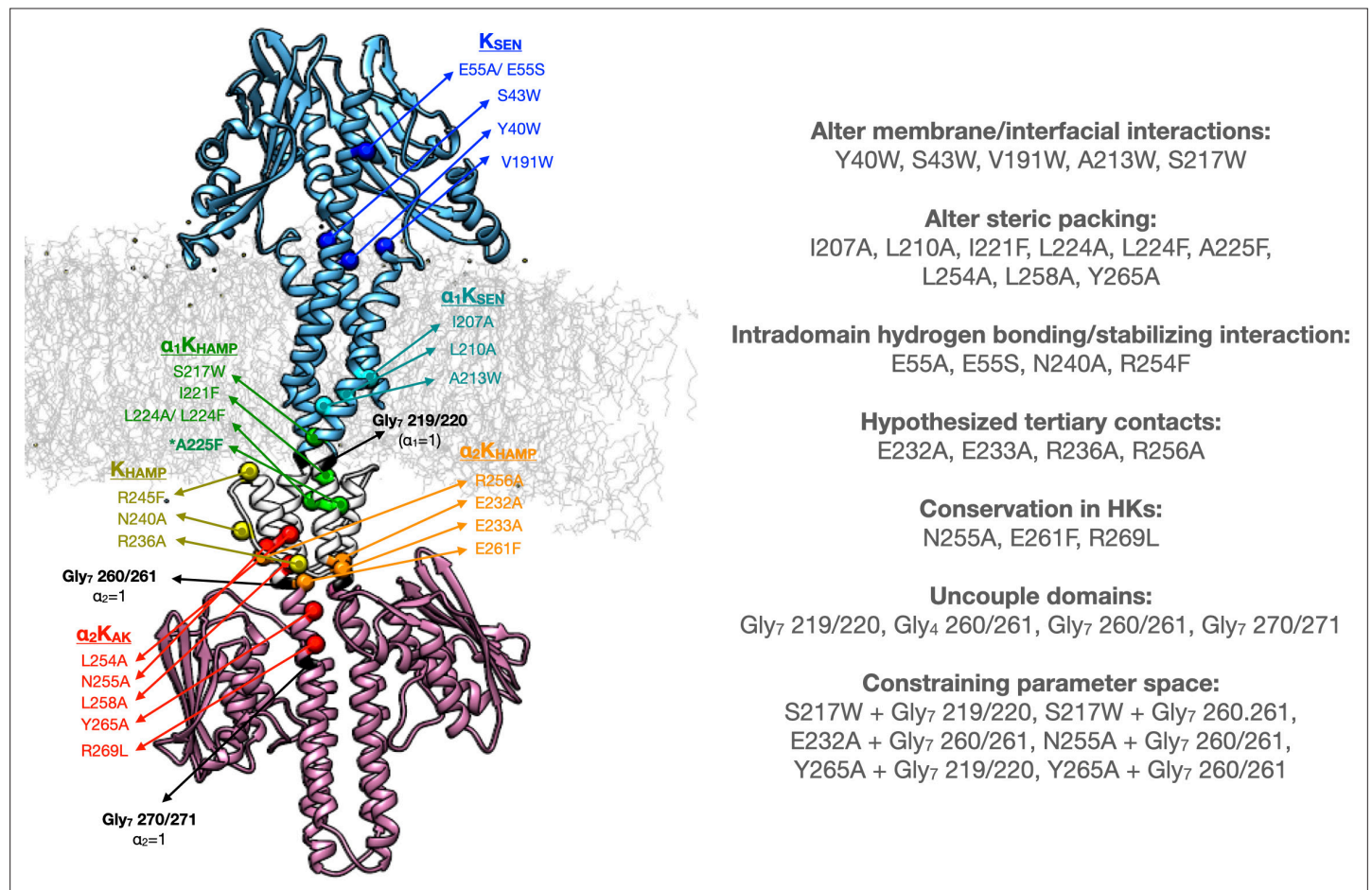


Figure 7—figure supplement 1. Point mutations and Gly7 insertions in PhoQ. A molecular dynamics model of PhoQ shows the location of mutations on one monomer with colored C β spheres. Colors correspond to mutation labels in **Figure 8**.

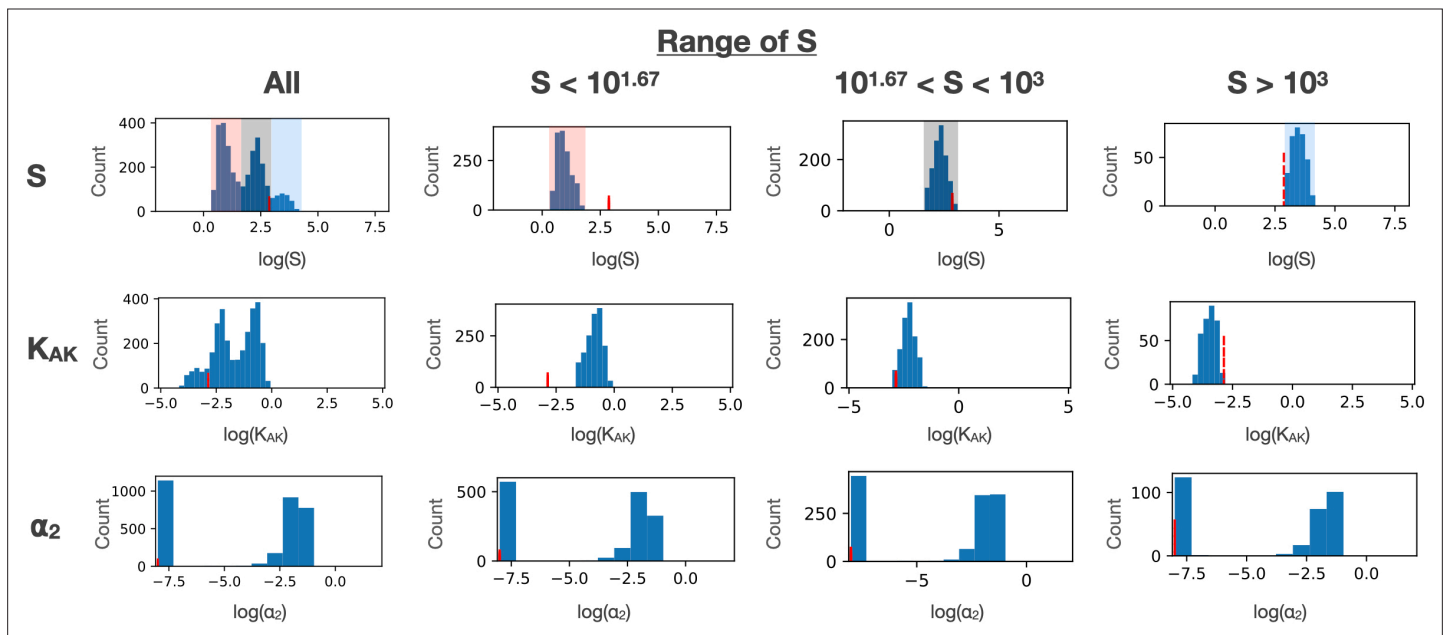


Figure 7—figure supplement 2. Effect of constraining S and K_{AK} . The confidence intervals for K_{AK} and α_2 parameters are shown as a function of different ranges of S values. S and K_{AK} show strong correlation.

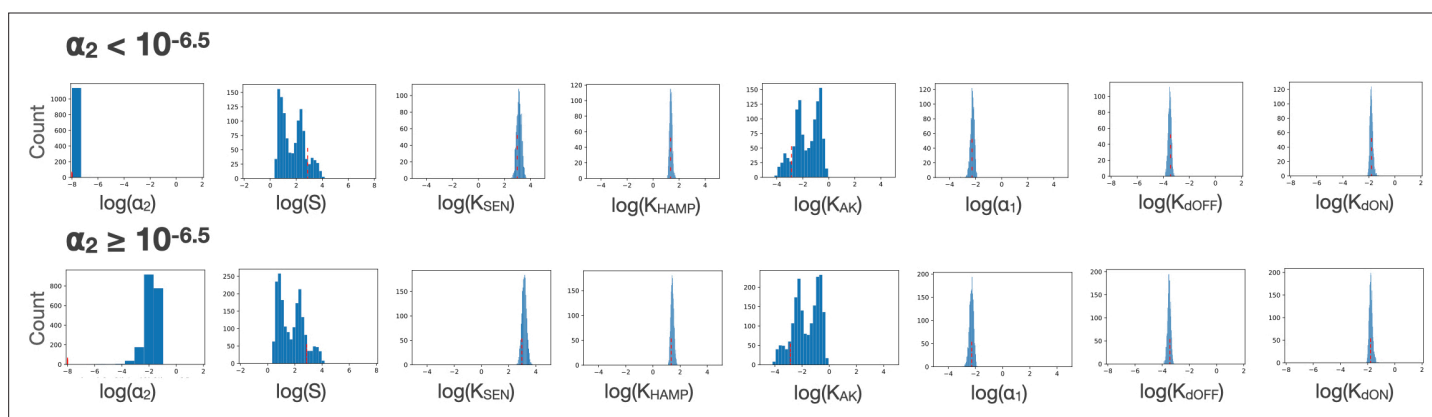


Figure 7—figure supplement 3. Effect of constraining α_2 . The confidence intervals for all global parameters are shown as a function of different ranges of α_2 values.

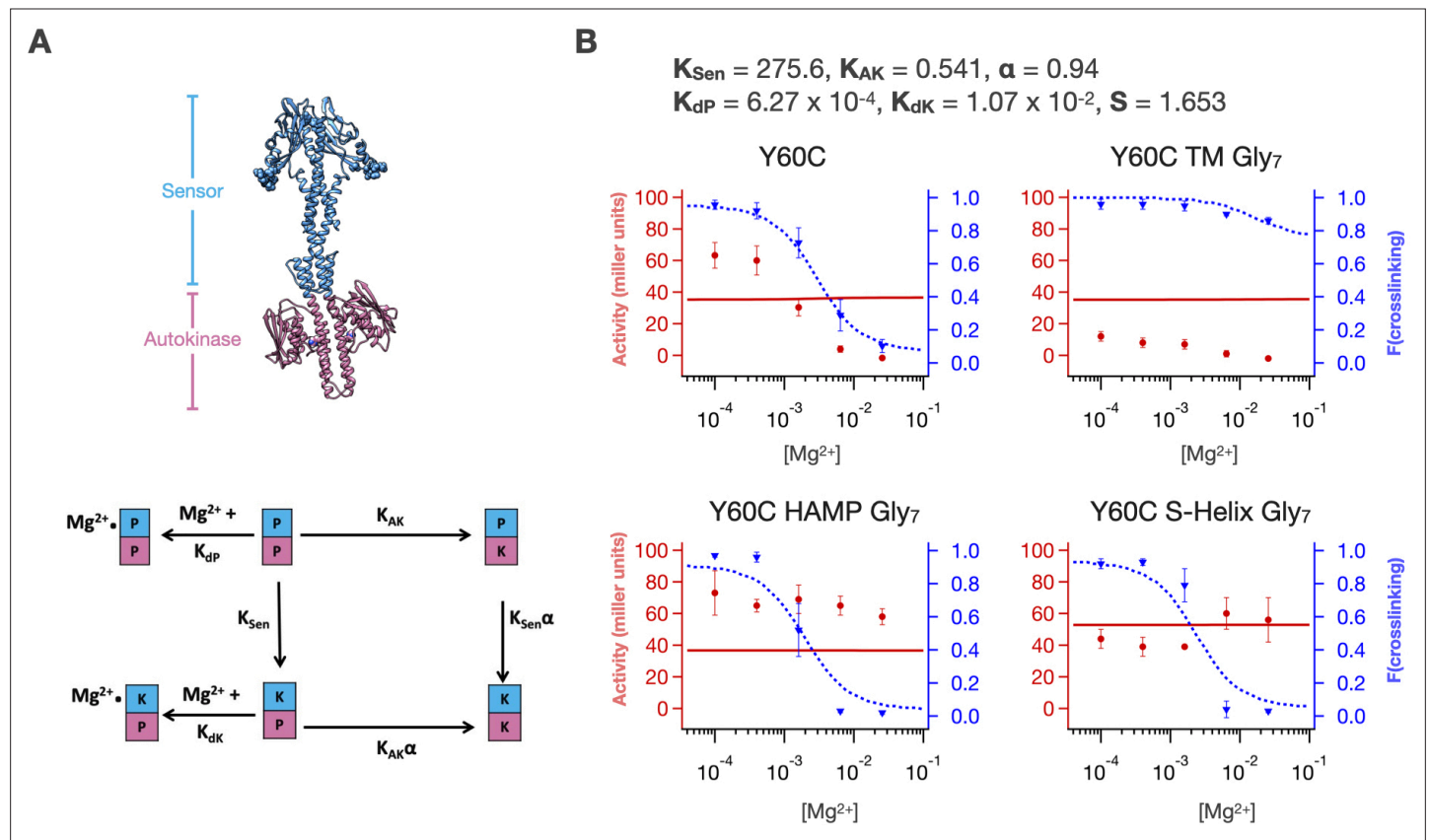


Figure 7—figure supplement 4. A two-domain two-state allosteric coupling model does not fit set of PhoQ mutants. **(A)** In a two-domain signaling model, PhoQ is split into two domains, the ‘Sensor’ which includes the periplasmic PAS domain, TM and HAMP domains, and the ‘Autokinase’. These two domains have their own intrinsic equilibria, K_{Sen} and K_{AK} , which are coupled in their ‘on’ states by the parameter α . The population ensemble is perturbed by Mg^{2+} binding to both states of the Sensor. **(B)** Global fitting of PhoQ single point mutant and Gly₇ insertion data set cannot simultaneously fit sensor crosslinking and autokinase activity data. Representative fits for WT phoQ and Gly₇ disconnections are shown.

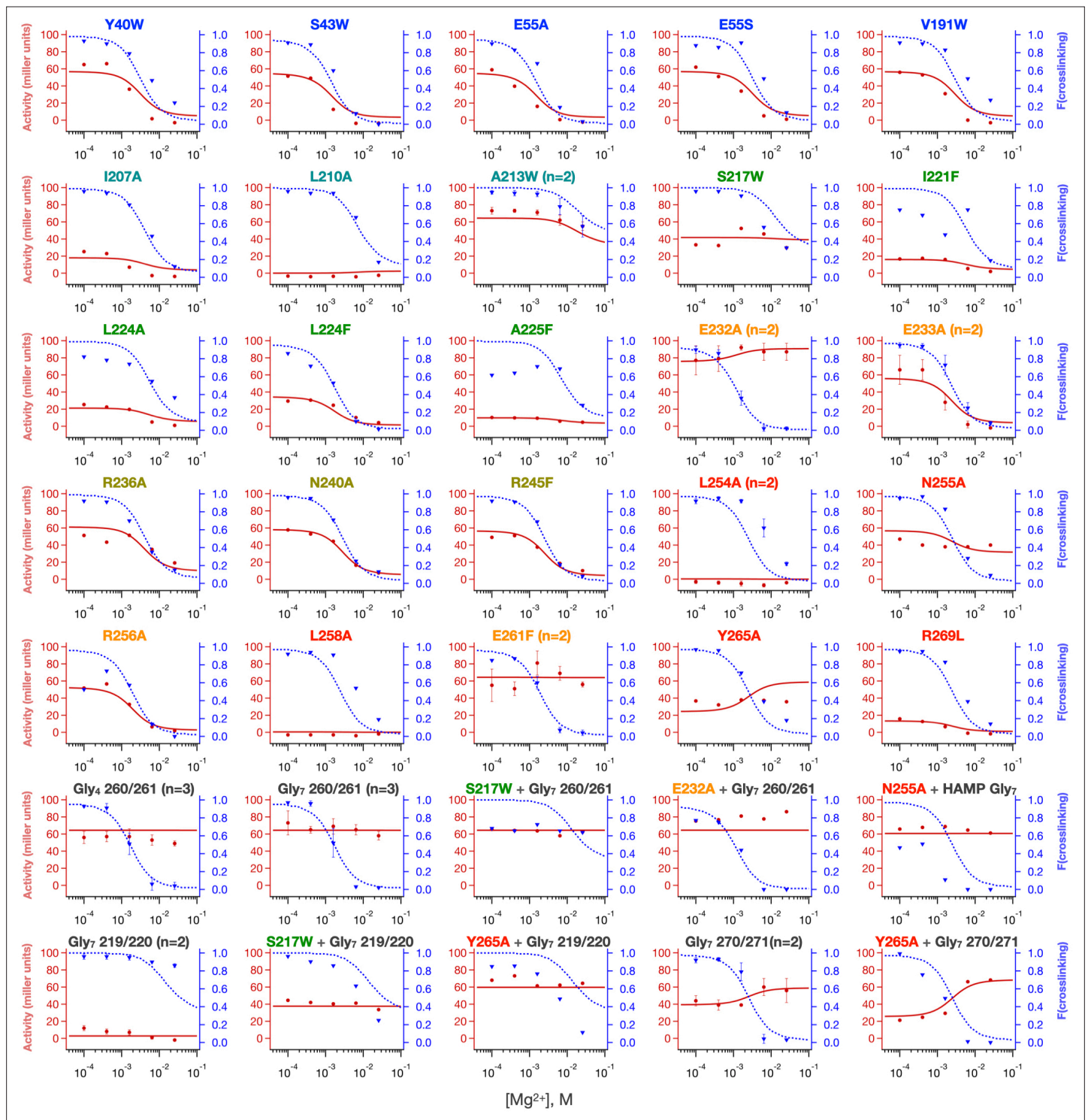


Figure 8. Local fits of sensor crosslinking and kinase activity for 35 PhoQ mutations. Fits to activity (red line, closed circles) and sensor crosslinking (blue dashed line, triangles) are shown for the entire PhoQ dataset. The color of mutations matches the color scheme in **Figure 7—figure supplement 1** to indicate locally varied parameters, and these parameters are listed in Table 1 and Table 2. Confidence intervals and residual sweep analyses are presented in **Figure 8—figure supplement 1**. Poor fits are highlighted in **Figure 8—figure supplement 2**.



Figure 8—figure supplement 1. Bootstrapped confidence intervals and residual sweep analyses for PhoQ mutant fits. Histograms from 3,061 convergent fits of simulated datasets for each local variable are shown in top panels. Residual sweeps in which the sum of residuals of the global fit is plotted as a function of indicated parameter being varied locally is shown in the bottom panels. Values of parameter fits are shown with red (x) and (y) marks.

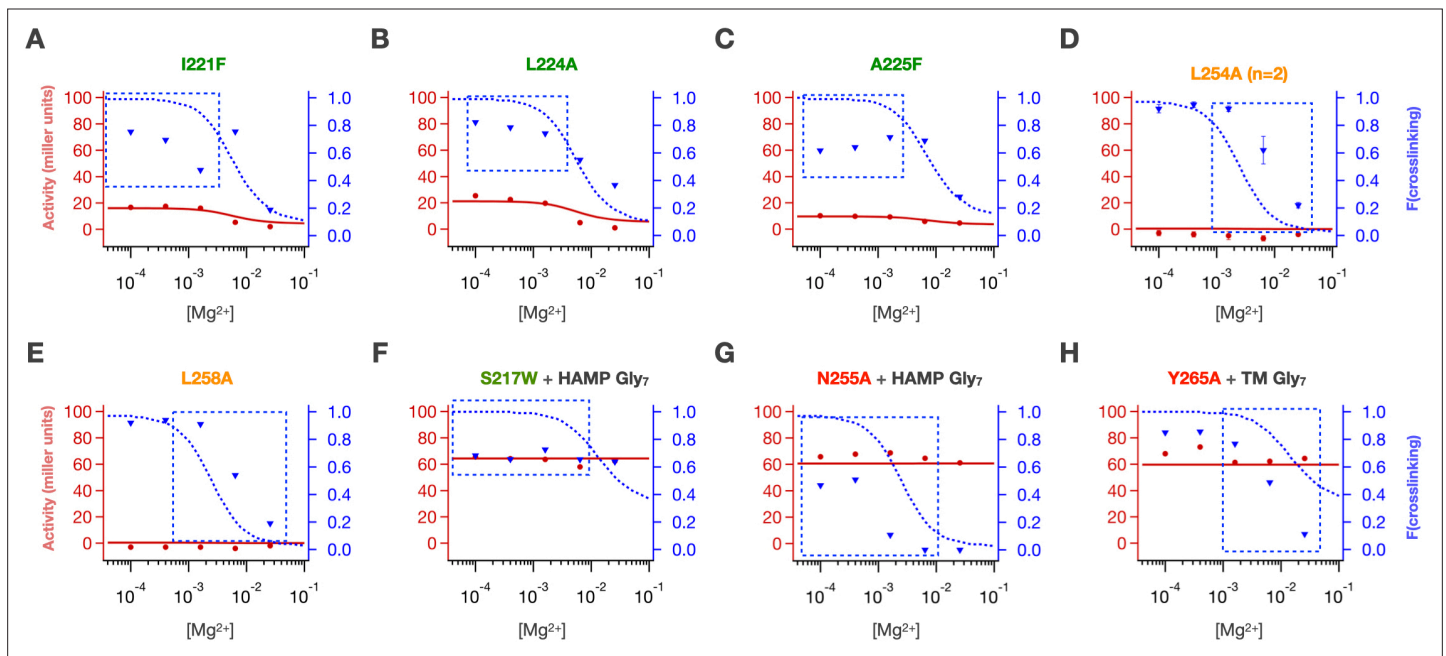


Figure 8—figure supplement 2. Poor fits were obtained for crosslinking at low $[Mg^{2+}]$ for (A) I221F, (B) L224A and (C) A225F. Poor midpoints of crosslinking transitions were fit for (D) L254A and (E) L258A. Some combinations of mutations had poor crosslinking fits (F) S217W + HAMP Gly₇, (G) N255A + HAMP Gly₇ and activity fits (H) Y265A + sensor Gly₇.

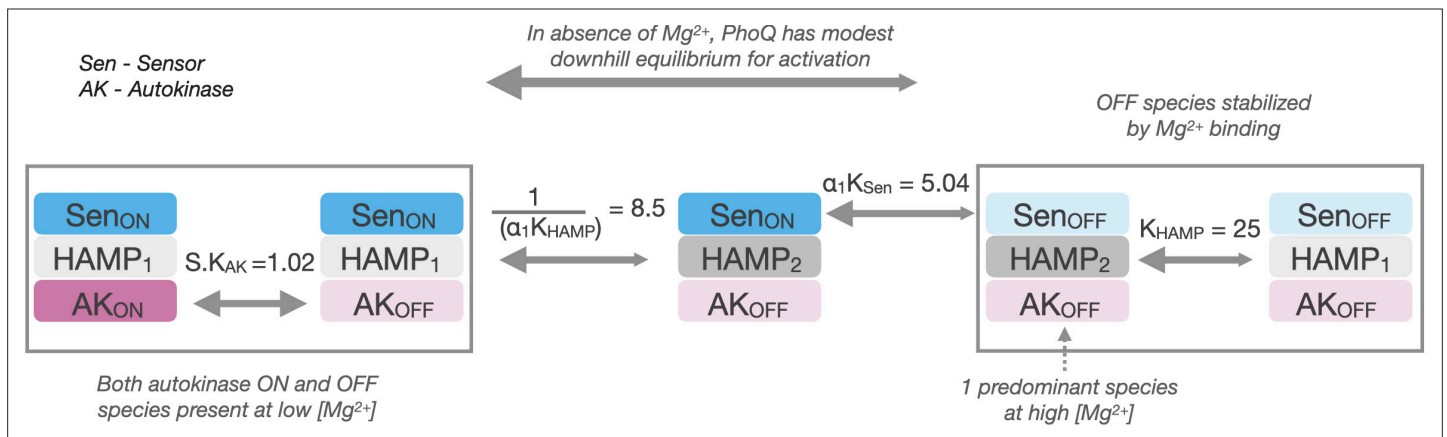


Figure 9. Allosteric pathway for PhoQ activation. In the absence of Mg^{2+} , PhoQ has a moderate downhill equilibrium to a mixture of active states. Mg^{2+} binding is sufficient for overpowering this equilibrium and stabilizing the 'kinase-off' state, resulting in a predominantly Sensor-off/HAMP2/Autokinase-off population.